Scanning Hall-probe microscopy system for two-dimensional imaging of critical current density in RE-123 coated conductors

Higashikawa, Kohei
Department of Electrical Engineering, Graduate School of Information Science and Electrical Engineering, Kyushu University

Inoue, Mitsuteru
Department of Electrical Engineering, Graduate School of Information Science and Electrical Engineering, Kyushu University

Kawaguchi, Toshikazu
Department of Electrical Engineering, Graduate School of Information Science and Electrical Engineering, Kyushu University

Shiohara, Kei
Department of Electrical Engineering, Graduate School of Information Science and Electrical Engineering, Kyushu University

他

出版情報：Physica C : Superconductivity and its Applications. 471 (21/22), pp.1036-1040, 2011-11. Elsevier
バージョン：

WTP-76 / ISS2010

Submitted 2 November 2010

Revised 27 December 2010

Scanning Hall-probe microscopy system for two-dimensional imaging of critical current density in RE-123 coated conductors

K. Higashikawa [a,*], M. Inoue [a], T. Kawaguchi [a], K. Shiohara [a], K. Imamura [a], T. Kiss [a],

Y. Iijima [b], K. Kakimoto [b], T. Saitoh [b],

T. Izumi [c]

[a] Department of Electrical Engineering, Graduate School of Information Science and Electrical Engineering, Kyushu University, 744 Motooka, Nishi-ku, Fukuoka 819-0395, Japan

[b] Material Technology Laboratory, Fujikura, 1-5-1, Kiba, Koto-ku, Tokyo 135-8512, Japan

[c] Superconductivity Research Laboratory, International Superconductivity Technology Center, 1-10-13 Shinonome, Koto-ku, Tokyo 135-0062, Japan

Abstract

We have developed a characterization method for two-dimensional imaging of critical current density in coated conductors (CCs) based on scanning Hall-probe microscopy (SHPM). The distributions of the magnetic field around a sample were measured for several different conditions of external magnetic fields, and then were converted to those of the sheet current density which flowed to shield the external magnetic field or to trap the penetrated magnetic field. As a result, it was found that the amplitude of the sheet current density corresponded to that of critical current density almost in all the area of the sample except for the region where current direction changed. This indicates that we could obtain an in-plane distribution of the critical current density with a spatial resolution of around 100 μm in non-destructive manner by this method. We believe that this measurement will be a multifunctional and comprehensive characterization method for coated conductors.

PACS codes: 74.25.Sv, 74.72.-h, 84.71.Mn

Keywords: coated conductor, critical current distribution, external magnetic field, scanning Hall-probe microscopy

* Corresponding Author.

Dr. Kohei Higashikawa

Postal address: Kiss Laboratory, Department of Electrical Engineering, Graduate School of Information Science and Electrical Engineering, Kyushu University, 744 Motooka, Nishi-Ku, Fukuoka 819-0395, Japan

Tel: +81-92-802-3678

Fax: +81-92-802-3677

E-mail: kohei@super.ees.kyushu-u.ac.jp

1. Introduction

Non-destructive characterization methods for investigating the homogeneity of critical current density in $REBa_2Cu_3O_{7-\delta}$ (REBCO, RE: rare earth) coated conductors (CCs) are indispensable for their further performance improvement and quality control necessary in the stage of industrial production. Magneto-optic imaging (MOI) [1, 2] is a powerful method for visualizing local inhomogeneity in CCs with a very good spatial resolution. TAPESTAR^{TM} [3, 4] is a well-known method for estimating longitudinal distribution of critical current in CCs. However, MOI may not be able to give a standardized calibration method for a quantitative characterization because of the individual variability of the indicator films and the photographing settings of brightness and contrast changed with measurement conditions. Furthermore, TAPESTAR^{TM} cannot give information about the inhomogeneity in the width direction of a CC with an enough spatial resolution, while such information is very important in processing for multifilamentary CCs as well as in cutting for finer CCs. Magnetoscan [5, 6] may overcome these problems. However, magnetoscan also needs a careful calibration for a quantitative characterization because the electromagnetic behavior in a sample strongly depends on the scanning speed, the distance between the sample and the permanent magnet and so on. For the compensation of these characterization methods, we developed a scanning Hall-probe microscopy system for two-dimensional imaging of critical current density in CCs in this study.

2. Methods

2.1. Measurement System

Fig. 1 shows the setup of the measurement system. The system has two liquid nitrogen tanks; one is for current leads, and the other is for a cooling stage. A sample together with a Bi-2223 coil used for external magnetic field to the sample was cooled by heat conduction from the cooling stage. Typical temperatures of them become the same as 79 K. The Hall probe is located above the sample. The active area of the Hall sensor is 50 μm x 50 μm, and perpendicular component of the magnetic field, B_z, is measured by this sensor. The Hall probe can be scanned with a spatial resolution of 1 μm, 1 μm and 0.25 μm in x, y and z directions, respectively. We measured distributions of the magnetic field around the sample for several different conditions of external magnetic field, and then converted them to those of sheet current density which flowed to shield the external magnetic field or to trap the penetrated magnetic field.

2.2. Sample

Fig. 2 shows the setup of the sample. We selected a sample from Fujikura Ltd. for this measurement. The sample was cut from a 10-mm-wide tape fabricated by reel-to-reel processes. The original tape had a critical current of 620 A at 77 K with respect to 2.5-μm-thick $GdBa_2Cu_3O_{7-\delta}$ layer deposited by pulsed laser deposition.

2.3. Data Analysis

Because of the distance between the Hall sensor and the superconducting layer, spatial harmonics are reduced in the distribution of measured magnetic field compared with the case of magnetic field just in the plane of superconducting layer, B_{z0}. Roth et al. reported a method for restoring the distribution of B_{z0} from that of B_z as follows [7]:

$$\widetilde{B}_{z0}(k_x, k_y) = e^{kz_{\text{lift-off}}} \widetilde{B}_z(k_x, k_y) \tag{1}$$

where $\widetilde{B}_z$ is the Fourier transformation of B_z. The variables k_x and k_y are the components of the wave number $\boldsymbol{k}$, and k is the absolute value of $\boldsymbol{k}$ given by $\sqrt{k_x^{\,2} + k_y^{\,2}}$. The constant $z_{\text{lift-off}}$ is the distance between the sensor and the superconducting layer of the sample. Furthermore, if we assume in-plane 2D current distribution in the sample, i.e., sheet current density in xy-plane, $\boldsymbol{J}$, the distribution of $\boldsymbol{J}$ can be derived analytically from that of measured B_z based on the inverse problem of Biot-Savart law. Roth et al. also reported a method for that, and x and y components of $\boldsymbol{J}$, J_x and J_y, are expressed as follows [7]:

$$\widetilde{J}_x(k_x, k_y) = -i \frac{2}{\mu_0} \frac{k_y}{k} e^{kz_{\text{lift-off}}} \widetilde{B}_z(k_x, k_y) \tag{2}$$

$$\widetilde{J}_y(k_x, k_y) = i \frac{2}{\mu_0} \frac{k_x}{k} e^{kz_{\text{lift-off}}} \widetilde{B}_z(k_x, k_y) \tag{3}$$

where $\widetilde{J}_x$ and $\widetilde{J}_y$ are the Fourier transformations of J_x and J_y, respectively. According to the increment of $z_{\text{lift-off}}$, spatial harmonics of $\widetilde{B}_z$ are weakened especially at large k. Eqs. (1), (2) and (3) indicate that such harmonics should be amplified by the term of $e^{kz_{\text{lift-off}}}$ to restore the magnetic field just at the current sheet. However, at very large k,

the harmonics are weakened down to a noise level of the measurement. This means that we should give up the information of such large k. We used a Hanning window, $w(k)$, as a low-pass filter:

$$w(k) = \begin{cases} \dfrac{1 + \cos\left(\dfrac{k}{k_{\text{cut-off}}} \pi \right)}{2} & \text{for } k \le k_{\text{cut-off}} \\ 0 & \text{for } k > k_{\text{cut-off}} \end{cases} . \quad (4)$$

The parameter $k_{\text{cut-off}}$ is the cut-off wavenumber, and the corresponding cut-off wavelength, $\lambda_{\text{cut-off}}$ (= 2π / $k_{\text{cut-off}}$), determines the spatial resolution of the obtained distribution of $\boldsymbol{J}$.

2.4. Procedure

After the sample was cooled down to 79 K in zero-field condition, the external magnetic field was increased from 0 mT to 105 mT. Furthermore, remanent magnetic field after the application of 120 mT was also measured.

3. Results and discussion

3.1. One-dimensional Distributions along the Width

Fig. 3 shows the measurement results on one-dimensional distributions of (a) the measured magnetic field, (b) the in-plane magnetic field and (c) the sheet current density along the width of the sample. The location was indicated by the arrow in Fig. 2,

and the results were obtained for several different conditions of external magnetic field, B_{ex}. It can be seen that the magnetic field penetrates from the edges of the sample as the external magnetic field increases. At $B_{ex} \sim 60$ mT, the magnetic field penetrates almost to the center of the sample. Similarly, the sheet current density was induced to shield the external magnetic field, and flowed largely from the edges of the sample. Such regions of the sheet current density spread from the edges to the center of the sample as the external magnetic field increases.

It should be noted that the amplitude of the sheet current density changes with the experienced magnetic field. When the amplitude of the sheet current density was plotted as a function of the experienced magnetic field on double logarithmic plot, we could obtain the graph shown in Fig. 4 (a). The graph shows the results for several different positions in the width direction. Furthermore, when the sheet current density was normalized by its value at $B_{z0} = 23$ mT, the normalized sheet current density, J_n, lied on the same curve independent of the position as shown in Fig. 4 (b). Then, the curve could be described very well by the following expression:

$$J(B_{z0}) = \begin{cases} \left(\dfrac{B_{z0}}{23\,\mathrm{mT}}\right)^{-0.05} J(23\,\mathrm{mT}) & \text{for } B_{z0} \le 23\,\mathrm{mT} \\ \left(\dfrac{B_{z0}}{23\,\mathrm{mT}}\right)^{-0.32} J(23\,\mathrm{mT}) & \text{for } B_{z0} > 23\,\mathrm{mT} \end{cases} . \quad (5)$$

To understand these phenomena, we also carried out a theoretical analysis on the assumption of critical state model [8]. When we supposed the critical current density, J_c,

to be a constant value of 40 A/mm, we could obtain the results shown in Fig. 5 (a). It can be seen that current flows at the amplitude of critical current density from the edges of the sample, and such region spreads almost to all the width of the sample except for the central position where current direction changes. Taking the condition of the remanent magnetic field for example, the current flows at the amplitude of critical current density except for 300-μm-wide region at the center of the 10-mm-wide sample. This means that we could estimate the distribution of critical current density almost in all the region of the sample in non-destructive manner by this method. However, the results in Fig. 5 (a) did not agree well with the measurement results in Fig. 3 (c).

On the other hand, when we consider the dependence of the magnetic field on the critical current density by Eq. (5), we could obtain the results shown in Fig. 5 (b). Furthermore, when their spatial resolution was matched to that of the measurement results, i.e., considering Eq. (4) with $\lambda_{\text{cut-off}} = 120$ μm, we could obtain the results shown in Fig. 5 (c). It can be seen that the theoretical results shown in Fig. 5 (c) agree very well with the measurement results shown in Fig. 3 (c). From this point of view, it could be concluded that we obtained the distribution of critical current density influenced by each experienced magnetic field. This means that we can also estimate the intrinsic distribution of critical current density, i.e., independent of the distribution of magnetic field in the sample, by considering the dependence of magnetic field on the critical current density such as Eq. (5).

3.2. Two-dimensional Distributions in the Plane

Fig. 6 shows the measurement results on two-dimensional distributions of the measured magnetic field, the in-plane magnetic field and the corresponding sheet current density in the sample. The results were obtained for a remanent magnetic field after the application of B_{ex} = 120 mT. The magnetic field is trapped in the sample, and the corresponding loop current flows in anticlockwise direction in the sample. As mentioned above, the amplitude of current density corresponds to the critical current density almost in all the area of the sample except for the region where current direction changes. From this point of view, it could be concluded that we could visualize two-dimensional distribution of critical current density in the sample by this method. Furthermore, considering the dependence of the magnetic field on the critical current density such as Eq. (5), we can also estimate an intrinsic distribution of critical current density independent of that of magnetic field. For example, the figure also shows the distribution of critical current density at B_{z0} = 23 mT. As a result, it can be seen that there are some defects in the sample while the distribution of critical current density is relatively uniform. We believe that these findings obtained by this measurement method will be very important for further performance improvement of CCs, processes for multifilamentary CCs for AC losses reduction and quality control necessary at industrial production.

4. Conclusion

We developed a characterization method for two-dimensional imaging of critical current density in CCs by means of scanning Hall-probe microscopy. We measured the distribution of magnetic field around the sample for several different conditions of external magnetic field, and converted them to the corresponding current distribution. It was found that the current flowed at the amplitude of critical current density almost in all the region of the sample for high enough external magnetic fields and for a remanent magnetic field after the application of high enough external magnetic fields. Furthermore, it was also found that we could estimate an intrinsic distribution of critical current density by considering the dependence of magnetic field on the critical current density. We believe that this measurement method will be a multifunctional and comprehensive characterization method for CCs.

Acknowledgments

This work was supported by the “New Energy and Industrial Technology Development Organization (NEDO) as the Project for Development of Materials & Power Application of Coated Conductors, M-PACC”, “JSPS: KAKENHI (20360143)” and “JSPS: KAKENHI (20.1945)”.

References

[1] T. H. Johansen, M. Baziljevich, H. Bratsberg, Y. Galperin, P. E. Lindelof, Y. Shen, P. Vase, Phys. Rev. B. 54 (1996) 16264.

[2] Ch. Jooss, R. Warthmann, A. Forkl, H. Kronmüller, Physica C 299 (1998) 215.

[3] Website of THEVA: http://www.theva.com/.

[4] S. Furtner, R. Nemetschek, R. Semerad, G. Sigl, W. Prusseit, Supercond. Sci. Technol. 17 (2004) S281.

[5] M. Eisterer, S. Haindl, T. Wojcik H. W. Weber, Supercond. Sci. Technol. 16 (2003) 1282.

[6] M. Zehetmayer, R. Fuger, M. Eisterer, F. Hengstberger, H. W. Weber, Appl. Phys. Lett. 90 (2007) 032506.

[7] B. J. Roth, N. G. Sepulveda, J. P. Wikswo Jr, J. Appl. Phys. 65 (1989) 361.

[8] E. H. Brandt, M. Indenbom, Phys. Rev. B 48 (1993) 12893.

Figure Captions

Fig. 1. Setup of the scanning Hall-probe microscopy system.

Fig. 2. Setup of the sample of a piece of 10-mm-wide $GdBa_2Cu_3O_{7-\delta}$ coated conductor.

Fig. 3. Measurement results on the distributions of (a) measured magnetic field, B_z, (b) in-plane magnetic field B_{z0}, and (c) sheet current density, J_x, along the width of the sample. The location is indicated in Fig. 2. The distributions were obtained for different conditions of external magnetic field, B_{ex}.

Fig. 4. (a) sheet current density, J, and (b) the normalized one, J_n, as a function of experienced magnetic field, B_{z0}, obtained for different width positions, y.

Fig. 5 Theoretical results on the distribution of sheet current density, J_x, along the width of the sample obtained from (a) critical state model, (b) the model considering Eq. (5), and (c) the model considering Eqs. (5) and (4). The distributions were obtained for different conditions of external magnetic field, B_{ex}.

Fig.6 Measurement results on the two-dimensional distributions of measured magnetic field, B_z, in-plane magnetic field B_{z0}, and sheet current densities, J_x, J_y, and J. Critical current density J_c for B_{z0} = 23 mT is also estimated in the figure.

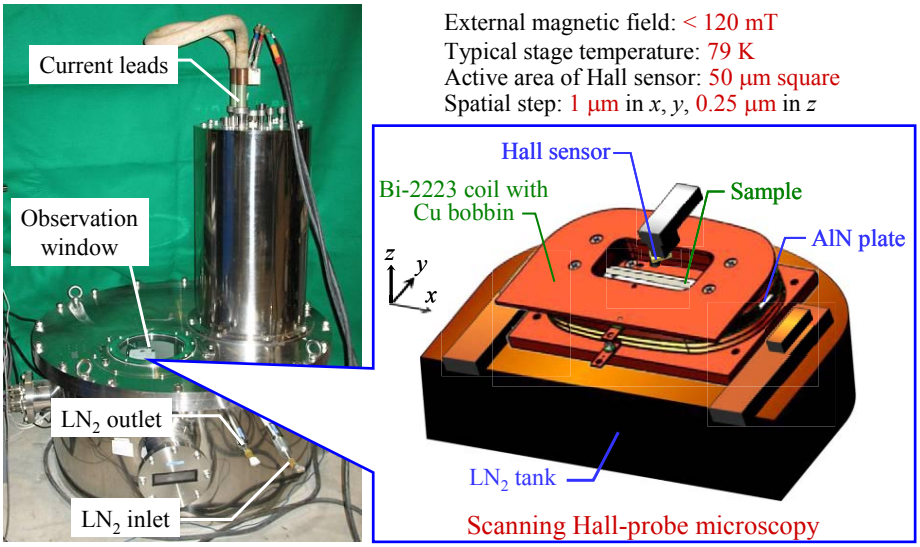
Current leads
Observation window
LN2 outlet
LN2 inlet
External magnetic field: < 120 mT
Typical stage temperature: 79 K
Active area of Hall sensor: 50 μm square
Spatial step: 1 μm in x, y, 0.25 μm in z
Hall sensor
Bi-2223 coil with Cu bobbin
Sample
AlN plate
z
y
x
LN2 tank
Scanning Hall-probe microscopy

Fig. 1

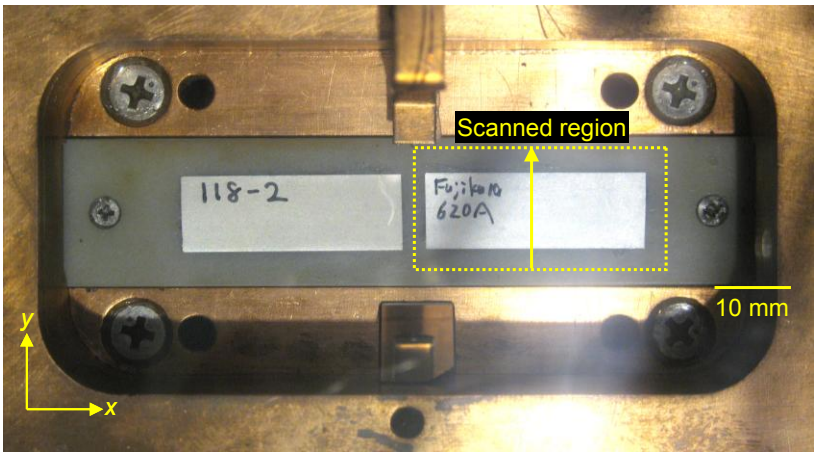
Scanned region
118-2
Fujikura
620A
10 mm
y
x

Fig. 2

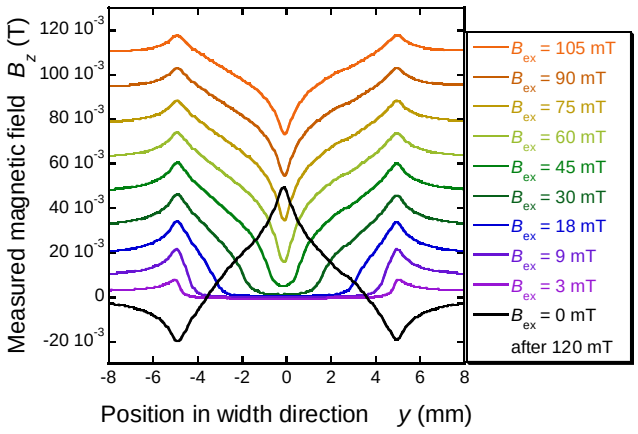
Measured magnetic field B_z (T)
120 10^{-3}
100 10^{-3}
80 10^{-3}
60 10^{-3}
40 10^{-3}
20 10^{-3}
0
-20 10^{-3}
-8 -6 -4 -2 0 2 4 6 8
Position in width direction y (mm)
B_{ex} = 105 mT
B_{ex} = 90 mT
B_{ex} = 75 mT
B_{ex} = 60 mT
B_{ex} = 45 mT
B_{ex} = 30 mT
B_{ex} = 18 mT
B_{ex} = 9 mT
B_{ex} = 3 mT
B_{ex} = 0 mT
after 120 mT

(a)

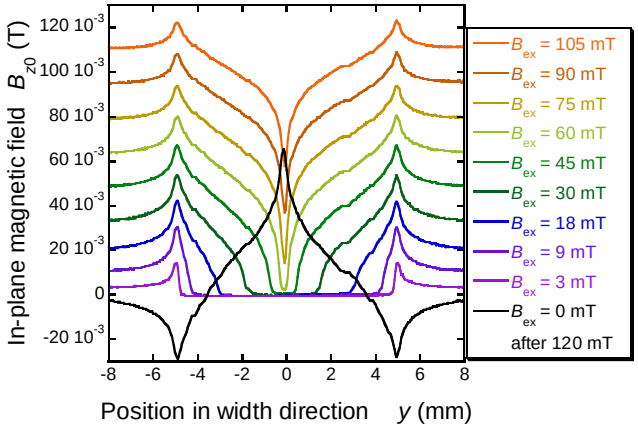
In-plane magnetic field B_{z0} (T)
120 10^{-3}
100 10^{-3}
80 10^{-3}
60 10^{-3}
40 10^{-3}
20 10^{-3}
0
-20 10^{-3}
-8 -6 -4 -2 0 2 4 6 8
Position in width direction y (mm)
B_{ex} = 105 mT
B_{ex} = 90 mT
B_{ex} = 75 mT
B_{ex} = 60 mT
B_{ex} = 45 mT
B_{ex} = 30 mT
B_{ex} = 18 mT
B_{ex} = 9 mT
B_{ex} = 3 mT
B_{ex} = 0 mT
after 120 mT

(b)

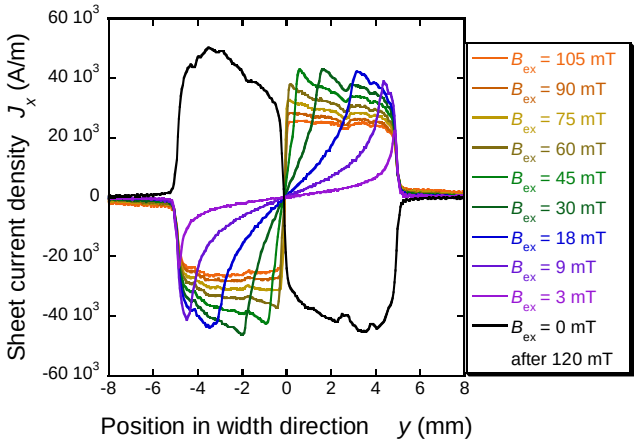
Sheet current density J_x (A/m)
60 10^3
40 10^3
20 10^3
0
-20 10^3
-40 10^3
-60 10^3
-8 -6 -4 -2 0 2 4 6 8
Position in width direction y (mm)
B_{ex} = 105 mT
B_{ex} = 90 mT
B_{ex} = 75 mT
B_{ex} = 60 mT
B_{ex} = 45 mT
B_{ex} = 30 mT
B_{ex} = 18 mT
B_{ex} = 9 mT
B_{ex} = 3 mT
B_{ex} = 0 mT
after 120 mT

(c)

Fig. 3

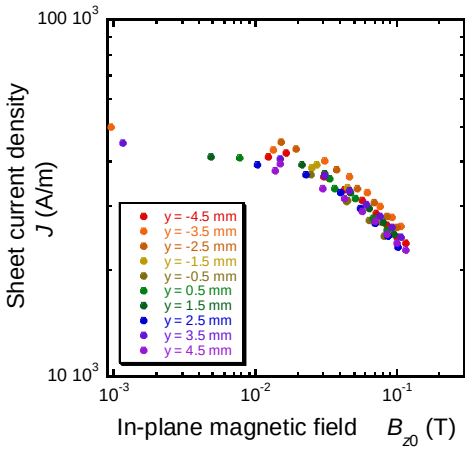
100 10^3
10 10^3
Sheet current density
J (A/m)
y = -4.5 mm
y = -3.5 mm
y = -2.5 mm
y = -1.5 mm
y = -0.5 mm
y = 0.5 mm
y = 1.5 mm
y = 2.5 mm
y = 3.5 mm
y = 4.5 mm
10^-3
10^-2
10^-1
In-plane magnetic field B_z0 (T)

(a)

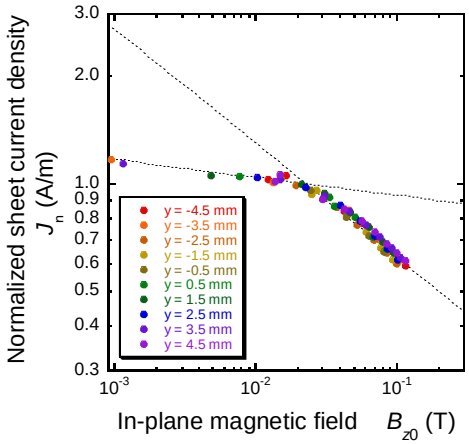
3.0
2.0
1.0
0.9
0.8
0.7
0.6
0.5
0.4
0.3
Normalized sheet current density
J_n (A/m)
y = -4.5 mm
y = -3.5 mm
y = -2.5 mm
y = -1.5 mm
y = -0.5 mm
y = 0.5 mm
y = 1.5 mm
y = 2.5 mm
y = 3.5 mm
y = 4.5 mm
10^-3
10^-2
10^-1
In-plane magnetic field B_z0 (T)

(b)

Fig. 4

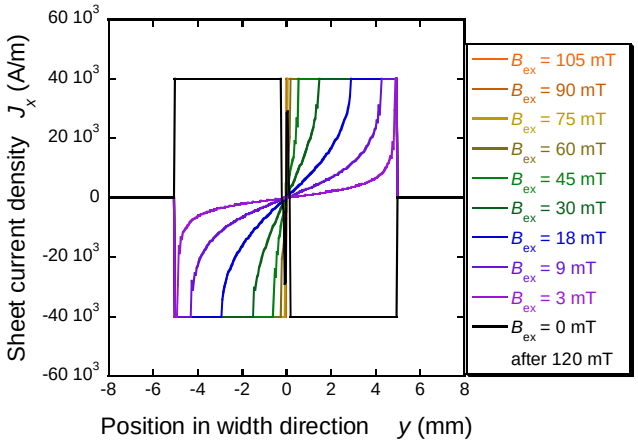
60 10^3
40 10^3
20 10^3
0
-20 10^3
-40 10^3
-60 10^3
Sheet current density J_x (A/m)
-8 -6 -4 -2 0 2 4 6 8
Position in width direction y (mm)
B_{ex} = 105 mT
B_{ex} = 90 mT
B_{ex} = 75 mT
B_{ex} = 60 mT
B_{ex} = 45 mT
B_{ex} = 30 mT
B_{ex} = 18 mT
B_{ex} = 9 mT
B_{ex} = 3 mT
B_{ex} = 0 mT
after 120 mT

(a)

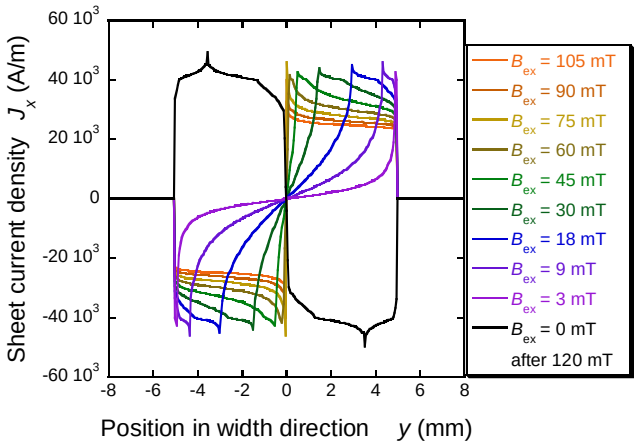
60 10^3
40 10^3
20 10^3
0
-20 10^3
-40 10^3
-60 10^3
Sheet current density J_x (A/m)
-8 -6 -4 -2 0 2 4 6 8
Position in width direction y (mm)
B_{ex} = 105 mT
B_{ex} = 90 mT
B_{ex} = 75 mT
B_{ex} = 60 mT
B_{ex} = 45 mT
B_{ex} = 30 mT
B_{ex} = 18 mT
B_{ex} = 9 mT
B_{ex} = 3 mT
B_{ex} = 0 mT
after 120 mT

(b)

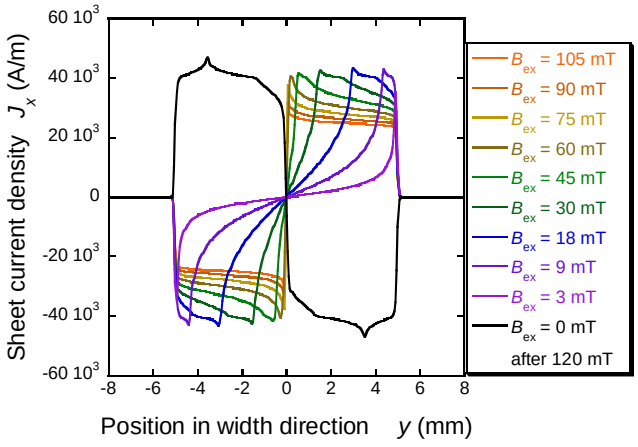
60 10^3
40 10^3
20 10^3
0
-20 10^3
-40 10^3
-60 10^3
Sheet current density J_x (A/m)
-8 -6 -4 -2 0 2 4 6 8
Position in width direction y (mm)
B_{ex} = 105 mT
B_{ex} = 90 mT
B_{ex} = 75 mT
B_{ex} = 60 mT
B_{ex} = 45 mT
B_{ex} = 30 mT
B_{ex} = 18 mT
B_{ex} = 9 mT
B_{ex} = 3 mT
B_{ex} = 0 mT
after 120 mT

(c)

Fig. 5

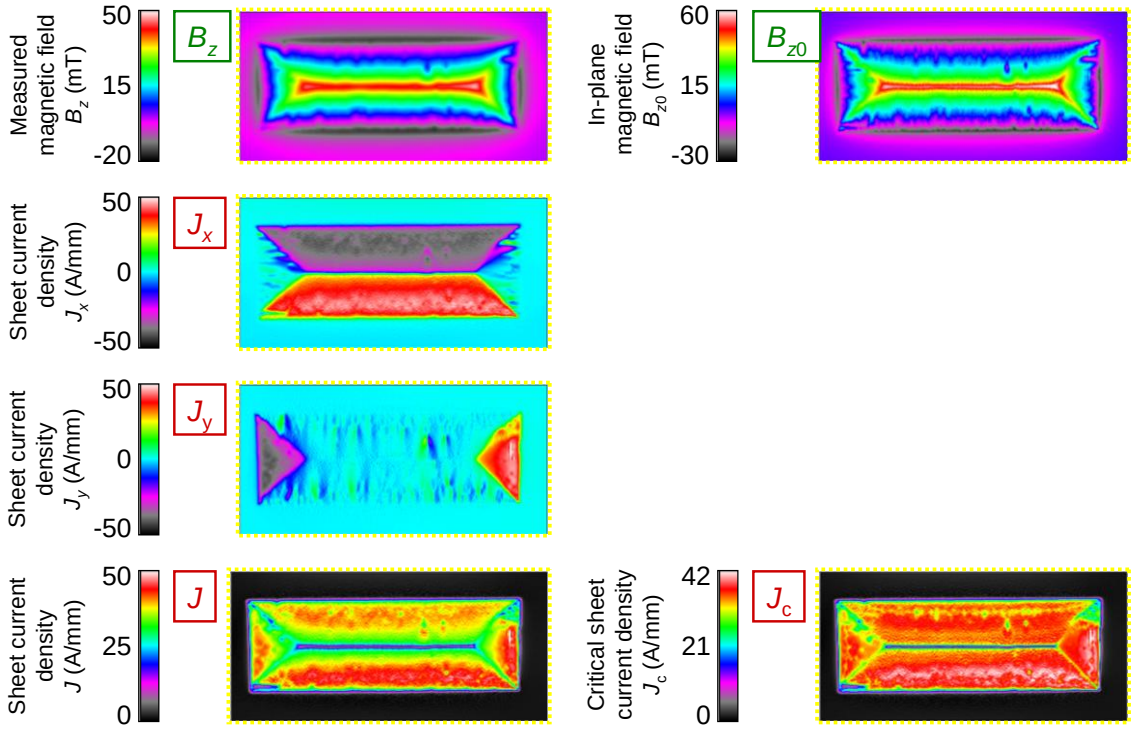
Measured magnetic field B_z (mT)
50
15
-20
B_z
In-plane magnetic field B_{z0} (mT)
60
15
-30
B_{z0}
Sheet current density J_x (A/mm)
50
0
-50
J_x
Sheet current density J_y (A/mm)
50
0
-50
J_y
Sheet current density J (A/mm)
50
25
0
J
Critical sheet current density J_c (A/mm)
42
21
0
J_c

Fig. 6